Research Paper

Low-Switching Based Improved PWM for Torque Harmonic Reduction in V/f Controlled High Power Inverter Fed IM Drive

Shivam Yadav [ID] *, Sanjeev Kumar Mallik* * [ID] *, Ambarisha Mishra* [ID]

Department of Electrical Engineering National Institute of Technology, Patna, Bihar, India.

Abstract— *Low Switching-based v/f-controlled induction motor (IM) drives are incredibly susceptible to torque harmonics and their Vibrations. These consequences lead to intensifying losses, damage drive, and can even turn out into shaft failure of high power/speed drives. In literature, numerous control algorithm based on pulse width modulation (PWM) has been reported for low switching-based IM drive. Nowadays, standard PWM techniques (Sinusoidal PWM ($S-PWM$), selective harmonic elimination (SHE) PWM) are being used as the solution in low-switching IM drives. In this manuscript, the proposed synchronous reference frame (SRF) based $P-PWM$ scheme is analytically evaluated to minimise the torque harmonics and its vibration in low switching IM drive. In this paper, a specific case of four switching angles per quarter cycle ($Sq=4$) is considered in which the optimized switching angles are obtained while maintaining the quarter wave symmetry (QWS) and half wave symmetry (HWS) nature of the waveform. The proposed approach is validated on $1hp$ IM drive and compared with $S-PWM$ and $SHE-PWM$ with respect to torque spectrum and vibration under No Load and different loading conditions. Real-time waveforms are recorded using the SRF-based $P-PWM$ technique and the $TYPHOON-HIL$ hardware setup to demonstrate the superior performance of the SRF-based $P-PWM$ in comparison to $S-PWM$ and $SHE-PWM$, in terms of lower torque harmonics and their vibrations.*

Keywords—IM drive, P- PWM, S-PWM, SHE-PWM, SRF-based PWM, Torque Vibration Minimization.

1. INTRODUCTION

The prevalent usage of popular electrical motors differs from everyday to manufacturing sectors, which are mainly controlled by applied voltage and frequency [1]. In electrical motors sectors, the induction motor (IM) dominates other motors due to numerous advantages, such as being rugged, robust, and economical [2]. Nevertheless, Presently, electrical drives are expanding at a rapid rate due to the optimized motion controlling of motors [3, 4]. High-power electrical drives are used in various sectors such as Oil, Mining, Air compressor, *etc.* [5].

As per the motor requirement, the power modulator of the drive performs energy modulation. In induction motor drives, the inverter is used as a power modulator that converts dc power into ac power [6]. Semiconductor devices used as switches of an inverter are arranged in a particular pattern, and their switching (ON/OFF) behaviour converts the dc power into distorted ac [7]. The inverter switching, controlled by suitable gate pulses, is generally based on the pulse variation known as Pulse Width Modulation (PWM) techniques [8, 9].

The inverter output develops a voltage in distorted sinusoids, comprising both fundament and harmonic components [9, 10]. The distorted harmonic voltage leads to harmonics in both, current and flux. The electromagnetic (EM) torque and its harmonics (torsional spectrum) are generated by the mutual interaction of harmonics in current and in flux. So, the EM-torque distorted waveform suffers mainly from lower-order EM torque harmonic measure and its steady state vibrations. IM drives with the pronounced amplitude of lower-order harmonics in torque trigger detrimental torsional oscillations, amplifying losses, inflicting damage on the drive system, and posing a severe risk of shaft failure.[11] Steady-state torque ripple in induction motor drives can lead to mechanical vibrations, reduced reliability and increased wear on motor components. It can also cause speed variations impacting the precision of applications and contribute to power losses as well as reduced energy efficiency [17].

Researchers have extensively explored various methods to reduce lower-order harmonics of electromagnetic torque (EM torque) in high-power drives [13]. These methods can be broadly classified into two categories: employing PWM algorithms for inverter gate signal generation and focusing on machine design improvements [14, 15]. Several PWM techniques have been reported by researchers in the literature, including standard PWM that comprises primarily $S-PWM$ and $SHE-PWM$ [12, 16]. Sinusoidal pulse width modulation ($S-PWM$) is a popular PWM technique based on the comparison between carrier and reference signals [18]. Another technique, selective harmonic elimination pulse width modulation ($SHE-PWM$) is also employed for pulse generation based on the solution of the non-linear equation and is prevalently used for the low switching frequency drive [19, 20]. These standard PWM techniques, Sinusoidal pulse width modulation ($S-PWM$) and selective harmonic elimination pulse width modulation ($SHE-PWM$) also suffer from certain limitations. $S-PWM$-based drives experience high switching losses, leading to reduced efficiency and increased power loss, as well as additional stress on power devices

that can result in heat generation, decreased reliability, and potential failures. Furthermore, the introduction of harmonic distortion in voltage and current waveforms leads to electromagnetic interference and compromises power quality [17, 20]. However, in order to address these switching losses, it is advantageous for high-power drives to operate at lower switching frequencies [10, 21]. On the other hand, $SHE - PWM$-based IM drives, frequently used for high-power drives are more sensitive to variations in machine parameters and have limited modulation index ranges, limiting their effectiveness in harmonic elimination [22, 23].

To address the above complex challenges and enhance the performance of high-power IM drives, synchronous reference frame (SRF) based $P - PWM$ methodology is proposed in this paper for the generation of gate pulses. This proposed approach aims to minimize EM lower-order torque harmonics and steady-state vibrations by optimizing the inverter's switching angles, taking into consideration of the coupling effect. The objective function along with constraints are being optimised to determine the optimal switching angle. The proposed approach even though maintains the quarter wave symmetry (QWS) and half wave symmetry (HWS) of the waveform and is also independent of machine and loading restrictions. Moreover, the proposed SRF-based $P - PWM$ method adopts a four-angle switching per quarter cycle ($sq = 4$) strategy, offering versatility for higher Sq and higher-order harmonics. The proposed method is validated using a $TYPHOON - HIL$-based hardware setup and compared with existing methods like $S - PWM$ and $SHE - PWM$.
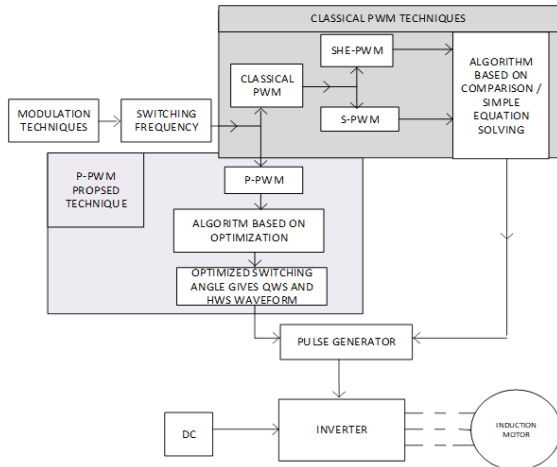

Fig. 1. Flowchart of inverter fed IM drive-based modulation techniques incorporating standard PWM and proposed SRF based $P - PWM$ approach.

2. STANDARD TORQUE ANALYSIS

IM drive is mainly governed by the nature of PWM techniques applied to the inverter. The overall procedure of this is depicted in Fig. 1. Generally, a low pulse number is preferred in high-power drives to limit switching losses [21]. The switching to fundamental frequency fraction is referred to as pulse number (P) related as ($P = (2Sq + 1)$) where Sq is the switching angle per quarter cycle. The fundamental component of voltage is varied only by one switching angle per quarter cycle ($Sq = 1$), although for harmonic alteration, more than one switching angle is vital ($Sq > 1$) [22].

An inverter-operated drive with ($Sq = 4$) is depicted here and standard torque harmonic analysis is performed. The fundamental odd-order harmonic voltage is given in (1) [23, 24]:

$$E_n = \frac{2E_{dc}}{n\pi}\left[1 + 2\sum_{k=1}^{sq}(-1)^k R_e e^{jn\alpha_k}\right] \quad (1)$$

Sq is switching per quarter, E_n denotes output voltage of nth harmonic, $0^0 \le \alpha_1 \le \alpha_2.......... \le \alpha_n \le 90^0$ condition satisfied by α_k Harmonic order denoted by n.

The voltage of the IM drive depends on current and flux with relation expressed in (2) [25, 27]:

$$E_n = RI_n + \frac{d\psi_n}{dt} \quad (2)$$

Where I, φ denotes current and flux, R is resistance, and Harmonic order is represented by n.

The occurrence of torque is attributed to the interaction between the constant $d - axis$ flux and the varying $q - axis$ current, as well as the interaction between the constant $d - axis$ current and the varying $q - axis$ flux. These interactions result in fluctuating torque values, and by addressing the variations in both the $d - axis$ and $q - axis$ components, the magnitude of torque ripple can be reduced.

Inverter-based IM drive is settled with ripples or vibrations in torque that are governed by the expression listed in (3) [21, 28]:

$$T = \left(\frac{P}{3}\right)[I_{d0}\psi_q - \psi_{d0}I_q - I_{q0}\psi_d] \quad (3)$$

Where the poles number is symbolized by P, 0 indicates the dc value, stator current and flux (d and q axis) indicated by I_d, I_q, φ_d and φ_q respectively.

The torque expression in (3), reveals the relationship between the $d - axis$ and $q - axis$ currents and fluxes, and the resulting torque in an induction motor. The occurrence of torque ripple, as described in the equation, is attributed to the interaction between the constant d-axis flux (φ_d) and the varying $q - axis$ current (I_q), as well as the interaction between the constant $d - axis$ current (I_d) and the varying $q - axis$ flux (φ_d).

Expressing stator currents (d and q axis) in terms of corresponding fluxes

$$I_d = \left(\frac{\psi_d}{L_{ls}}\right) \quad (4)$$

$$I_q = \left(\frac{\psi_q}{L_{ls}}\right) \quad (5)$$

Considering no load conditions ($I_{q0} = 0$) torque vibration stated in Equation (6) [25, 26]:

$$T = \left(\frac{P}{3}\right)\left[I_{d0} - \frac{\psi_{d0}}{L_{ls}}\right]\psi_q = C\psi_q \quad (6)$$

The proportionality constant C in (6) is $1.84/Lls$ where L_{ls} is leakage inductance of the motor. The calculation of flux vibration components (d and q axis) is related to corresponding voltage respectively stated in (7) and (8):

$$\frac{d}{dt}\psi_d = E_d \quad (7)$$

$$\frac{d}{dt}\psi_q = E_q \quad (8)$$

Similarly, the nth torque (T_n) harmonic component proportionate to φ_{qn} which depends on voltage amplitude (E_{qn}).

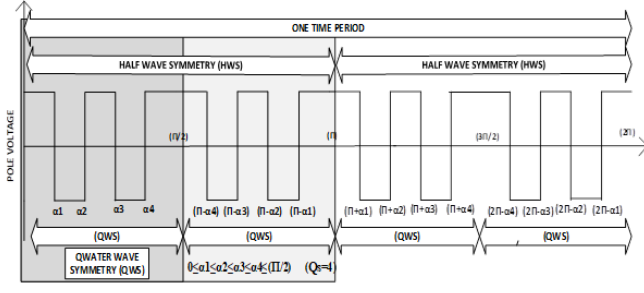$$T_n = k\psi_{qn} = k\frac{E_{qn}}{n\omega} \quad (9)$$

Fig. 2. Waveform principle for inverter pole voltage in IM drive for four switching angles per quarter.

2.1. Proposed SRF-based P-PWM

For low pulse numbers, $SRF - based$ method is proposed in this present section for minimizing the amplitude and vibration of torque harmonic in inverter-fed IM drive.

The flux vibration (d and q axis) is stated in (10) and (11), where ω is speed (synchronous) in rad/s.

$$\frac{d}{dt}\psi_d = -\omega\psi_q + E_d \qquad (10)$$

$$\frac{d}{dt}\psi_q = \omega\psi_d + E_q \qquad (11)$$

In standard analysis, the coupling effect stands neglected, but in low pulse analysis, the coupling effect, *i.e.*, cross-coupling, plays a significant role and can't be overlooked.

The expression of the $d-axis$ flux stated in (10) is differentiated and expressed in (12). Further, the value of $\frac{d}{dt}\psi_d$ is replaced in (12) from (10) and expressed in (13):

$$\frac{d^2}{dt^2}\psi_q = \omega\frac{d}{dt}\psi_d + \frac{d}{dt}E_q \qquad (12)$$

$$\frac{d^2}{dt^2}\psi_q = -\omega^2\psi + \omega E_d + \frac{d}{dt}E_q \qquad (13)$$

The expression expressed in (13) is rewritten for the nth harmonic component and stated in (14):

$$\frac{d^2}{dt^2}\psi_{qn} = -\omega^2\psi_n + \omega E_{dn} + \frac{d}{dt}E_{qn} \qquad (14)$$

Moreover E_{dn}, E_{qn},φ_{qn} be expressed in relation as mentioned in (15)-(17) having peak values and phase angle as E_{dmn}, E_{qmn}, ψ_{qmn} and $\phi_{E_{dn}}$, $\phi_{E_{qn}}$, $\phi_{\psi_{qn}}$ respectively.

$$E_{dn} = E_{dmn}\sin\left(n\omega t + \phi_{E_{dn}}\right) \qquad (15)$$

$$E_{qn} = E_{qmn}\sin\left(n\omega t + \phi_{E_{qn}}\right) \qquad (16)$$

$$\psi_{qn} = \psi_{qmn}\sin\left(n\omega t + \phi_{\psi_{qn}}\right) \qquad (17)$$

The detailed expression obtained by Substituting (15)-(17) into (14) is listed in (18):

$$n^2\omega^2\psi_{qmn}\sin\left(n\omega t + \varphi_{\psi qn}\right) = \omega^2\psi_{qmn}\sin\left(n\omega t + \varphi_{\psi qn}\right) - \omega E_{dmn}\sin\left(n\omega t + \varphi_{Edn}\right) - n\omega E_{qmn}\cos\left(n\omega t + \varphi_{Eqn}\right) \qquad (18)$$

$$\left(n^2 - 1\right)\omega^2\psi_{qmn}\sin\left(n\omega t + \varphi_{\psi qn}\right) = -\omega E_{dmn}\sin\left(n\omega t + \varphi_{Edn}\right) - n\omega E_{qmn}\cos\left(n\omega t + \varphi_{Eqn}\right) \qquad (19)$$

Meanwhile, for torque harmonic order $n^2 \gg 1$. Rearranging the left side term of (18), the expression can be considerably observed that in (19), the term $\left(n^2 - 1\right) \approx n^2 \gg 1$. Concludingly, the first term in (14) remains neglected. After that, the entire equation reduces to the voltage ($d - q$ reference frame) dependent expression stated in (20):

$$\frac{d^2}{dt^2}\psi_q \approx \omega E_d + \frac{d}{dt}E_q \qquad (20)$$

The harmonic voltages E_{dn} and E_{qn} expressed in orthogonal components as listed in (21) and (22) in which E_{dn} and E_{qn} corresponds the E_{nb1}, E_{na1} and E_{nb2}, E_{na2} as the amplitude of cosine and sine components.

$$E_{dn} = E_{na1}\sin\left(n\omega t\right) + E_{nb1}\cos\left(n\omega t\right) \qquad (21)$$

$$E_{qn} = E_{na2}\sin\left(n\omega t\right) + E_{nb2}\cos\left(n\omega t\right) \qquad (22)$$

The nth harmonic $q - axis$ flux vibration from (16) and (20) is expressed in (23):

$$\psi_{qn} = \frac{1}{n\omega}\left[\left(\left(E_{nb2} - \frac{E_{na1}}{n}\right)\sin\left(n\omega t\right)\right) - \left(E_{na2} + \frac{E_{nb1}}{n}\right)\cos\left(n\omega t\right)\right] \qquad (23)$$

Torque vibrations for high values of n are listed in (24):

$$T_n = \frac{k}{n\omega}\sqrt{\left(E_{na2} + \frac{E_{nb1}}{n}\right)^2 + \left(E_{nb2} - \frac{E_{na1}}{n}\right)^2} \qquad (24)$$

The same torque vibration expression in (24) can be reduced to (9) and rewritten herein (25) for the sake of convenience:

$$T_n = k\psi_{qn} = k\frac{E_{qn}}{n\omega} \qquad (25)$$

2.2. MINIMIZATION PROCEDURE FOR THE PROPOSED METHOD

The torque harmonics minimization procedure is generalised for inverter-fed IM drive, which includes objective function (OF) minimization stated in (26) with two primary constraints ($C1, C2$), namely modulation index (Mo) and angles per quarter stated in (27) and (28):

$$(OF)\, E_n = \left\|\left(\frac{E_{n-1}}{n - 1} + \frac{E_{n+1}}{n + 1}\right)\right\| \qquad (26)$$

$$(C1)\, Mo = 1 + \sum_{n=1}^{\infty}\left(-1\right)^n 2\cos\left(\alpha_n\right) \qquad (27)$$

$$(C2)\, 0^0 \leq \alpha_1 \leq \alpha_2 \leq \cdots\, ...\, ...\, ...\, \alpha_n \leq 90^0 \qquad (28)$$

This generalised form of the process of minimization is effective both for Sq and harmonic order. They are intended to validate the above-proposed method, the IM drive having $Sq = 4$, generating the lowermost torque harmonic of the 12th order that is minimized in the below sections.

2.3. Minimization for 12th-order torque harmonic

The 11th and 13th-order harmonic voltages are accountable for developing the 12th-order torque harmonic. Accordingly, the voltage-dependent objective function (OF) for its minimization will be stated in Equation (29) with constraints $(C1)$ and $(C2)$ for Mo and four switching angles per quarter in (30) and (31), respectively. Additionally, the constraint $(C3)$ here is expressed for 12th-order torque harmonic elimination denoted in (32):

$$(OF)\, E_{12} = \left\| \left(\frac{E_{11}}{11} + \frac{E_{13}}{13} \right) \right\| \qquad (29)$$

$$(C1)\, Mo = 1 - 2 * \cos\alpha_1 + 2 * \cos\alpha_2 - 2 * \cos\alpha_3 + 2 * \cos\alpha_4 \qquad (30)$$

$$(C2)\, 0^0 \le \alpha_1 \le \alpha_2 \le \alpha_3 \le \alpha_4 \le 90^0 \qquad (31)$$

$$(C3)\left(\frac{E_{11}}{11} = \frac{E_{13}}{13} \right) \qquad (32)$$

The proposed SRF-based $P-PWM$ approach in inverter-fed IM drive is based on the solution of an optimization problem with objective function and constraints. The computation of the optimised problem results in four optimised switching angles $(\alpha_1, \alpha_2, \alpha_3, \alpha_4)$ and is effectively used for torque vibration and harmonic magnitude reduction.

The proposed approach procedure is simple, quick and further, easily extendable for higher torque harmonics and Sq.

The algorithm-based optimised switching angles produce switching signals. Further, these signals termed pulse generators, are fed to the gate terminal of the inverter. The switches of the inverter are ON/OFF in a particular fashion in accordance with an algorithm to generate a voltage at inverter terminals. The generated line voltage waveform per cycle maintains QWS (quarter wave symmetry) and HWS (half wave symmetry). The waveform operating principle of pole voltage with $(Sq = 4)$, resulting pulse number $(P = 9)$ shown in Fig. 2. The line and phase voltage waveforms composed of fundamental and other harmonics, are responsible for generating the current and flux waveforms. The minimized torque harmonics are generated by the interaction of current and flux (fundamental and harmonic) expressed in (3).

3. RESULTS ANALYSIS

The inverter fed $1hp$, $1440rpm$, $415V$, $50Hz$ IM drive is implemented in $TYPHOON-HIL$, and results are attained with parameters of IM listed in Table 1. The $TYPHOON-HIL$, when linked to a computer, passes on gate signals to the inverter through a gate-triggering circuit and related wiring. The inverter, in response, operates the induction motor. The voltage and current readings are captured and processed through HIL-Connect. These voltage and current signals are then utilized to determine the torque profile of the induction machine in the $TYPHOON-HIL$ and the resulting waveforms are presented in a digital storage oscilloscope (DSO) for harmonic spectrum analysis. The $TYPHOON-HIL$-based hardware setup is illustrated in Fig. 3. The drive has been executed at $Sq = 4$ in $TYPHOON-HIL$, and results are obtained, both at no load and loading conditions. The relative analysis of the inverter-fed IM drive is performed for diverse PWM techniques, primarily including standard PWM $(S-PWM, SHE-PWM)$ and proposed SRF-based $P-PWM$. The analysis of various aspects of the drive such as inverter performance, torque vibrations and spectrum are listed in the forthcoming sections.
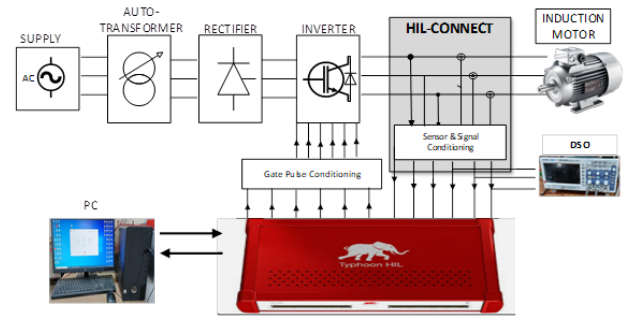
(a)
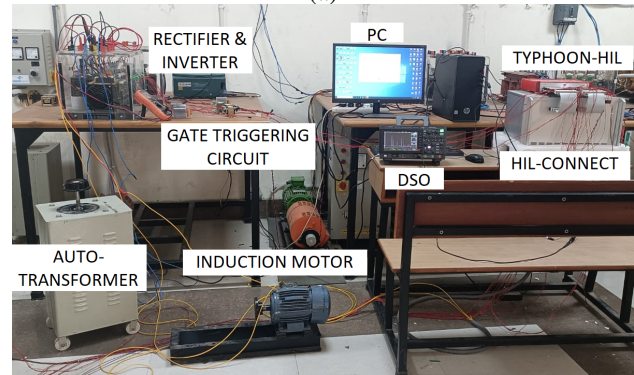
(b)

Fig. 3. Connection Diagram (a) Block Diagram (b) Hardware Setup.

3.1. INVERTER PERFORMANCE ASSESSMENT

For diverse modulation techniques, the inverter performance of IM Drive has been analysed. The performance of the inverter-operated PWM algorithms has been assessed from its output waveforms and shown in Fig. 4 and Fig. 5. The drive is simulated for No load condition, and inverter output waveforms for $S-PWM$, $SHE-PWM$, and SRF-based are depicted in Fig. 4. and DSO sensed waveforms output in Fig. 5, respectively.

In an $S-PWM$-based IM drive, for $Sq = 4$ the Line voltage is shown in Fig. 4-(a). and DSO measured line voltage in Fig. 5-(a). The Line voltage is deprived of symmetrical nature, hence QWS and HWS nature of the waveform is not maintained. It also divulges in Fig. 4-(b) and Fig. 5-(b). of the voltage spectrum which shows the presence of lower 6th order harmonic corresponding to $300Hz$, 10th order harmonics corresponding to $500Hz$ further, 15th order harmonics corresponding to $750Hz$ respectively. Higher-order harmonics are not taken into consideration. Hence, it shows the presence of both odd and even order harmonics as QWS and HWS waveform nature is not maintained in the voltage spectrum in $S-PWM$-based IM drive.

Alternatively, for $Sq = 4$ in $SHE-PWM$-based IM drive, the Line voltage of inverter outputs are shown in Fig. 4-(c) and DSO sensed waveform in Fig. 5-(c). It depicts that symmetrical nature is maintained in line voltage consequently, they are also QWS and HWS. Further, the voltage spectrum is shown in Fig. 4-(d) and Fig. 5-(d)., which describes the presence of (11th and 13th) order harmonics corresponding to ($550Hz$ and $650Hz$) as the lowermost harmonic in the above-mentioned drive having four switching angles per quarter.

Further, SRF-based $P-PWM$ inverter-fed IM drive ensures the symmetrical nature of the waveform in both Line Voltage and sensed voltage in DSO as depicted in Fig. 4-(e) and Fig. 5-(e). The Real-time Line voltage waveform and its spectrum are illustrated in Fig. 4-(e) and Fig. 4-(f). The voltage spectrum contains only odd-order harmonics as QWS, HWS and the symmetrical nature of line voltage are maintained, and even order harmonics are
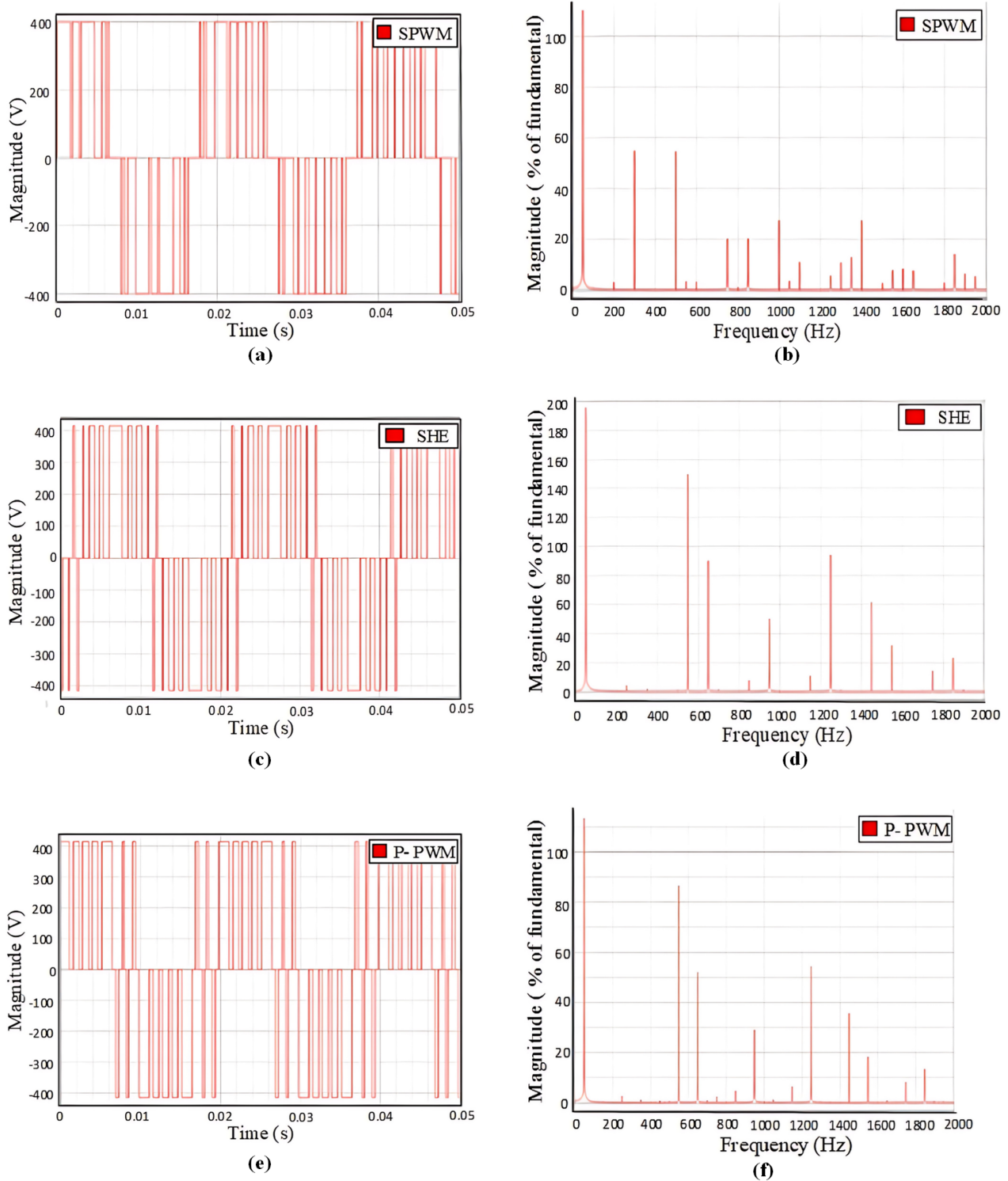
Fig. 4. Real-time Waveforms obtained from TYPHOON-HIL (a) $S-PWM$ Voltage (b) FFT of $S-PWM$ Voltage (c) $SHE-PWM$ Voltage (d) FFT of $SHE-PWM$ Voltage (e) $P-PWM Voltage$ (f) FFT of $P-PWM$ Voltage.

eliminated due to the HWS nature of the waveform. The spectrum of voltage in Fig. 4-(f). depicts the presence of the lowermost harmonic of the 11th order corresponding to $550Hz$ followed by the 13th order corresponding to $650Hz$.

The $S-PWM$-based IM drive shows the presence of odd and even harmonics (6th, 10th and 15th) due to the non-symmetrical nature of waveform shown in Fig. 4-(b), while $SHE-PWM$

and SRF-based $P-PWM$ IM drive has lowermost pair of (11th and 13th) order harmonics shown in Fig. 4-(d) and Fig. 4-(f). So, predominantly comparability lies within $SHE-PWM$ and SRF-based $P-PWM$, the voltage spectrum reveals that the magnitude of harmonics in SRF-based $P-PWM$ is lesser when compared to $S-PWM$ and $SHE-PWM$-based inverter-fed IM drive.

Fig. 5. Sensed Waveforms in DSO (a) $S-PWM$ Voltage (b) FFT of $S-PWM$ Voltage (c) $SHE-PWM$ Voltage (d) FFT of $SHE-PWM$ Voltage (e) $P-PWM$ Voltage (f) FFT of $P-PWM$ Voltage.

3.2. TORQUE PROFILE ASSESSMENT

The Steady-state torque is composed of vibrations that are produced mainly with the interaction of the harmonic current with fundamental flux and that of fundamental current with harmonic flux. Additionally, the modulation index has a significant impact on torque ripple, as excessive modulation can result in vibrations and decreased reliability. The optimal range of the modulation index (Mo) typically varies between 0 and 1. A higher modulation index can lead to increased switching losses and reduced efficiency, while a lower modulation index may restrict torque and speed capabilities.

The vibration analysis of torque in the present section is categorised in two cases, Case1 and Case2 for No load Condition

and 60% Loading condition respectively. Both the cases of inverter-fed IM drive have been executed in $TYPHOON-HIL$ and steady-state torque vibrations are shown in Fig. 6 and Fig. 7. with their corresponding measurements listed in Table 2 and Table 3 for different PWM techniques. Moreover, the vibrational performance of the IM drive has been evaluated using both the proposed and standard techniques within the optimal modulation index range. The measurements have been presented in Table 4. The analysis demonstrates that the SRF-based $P-PWM$ technique exhibits significantly lower vibrations compared to other PWM techniques ($S-PWM$ and $SHE-PWM$).
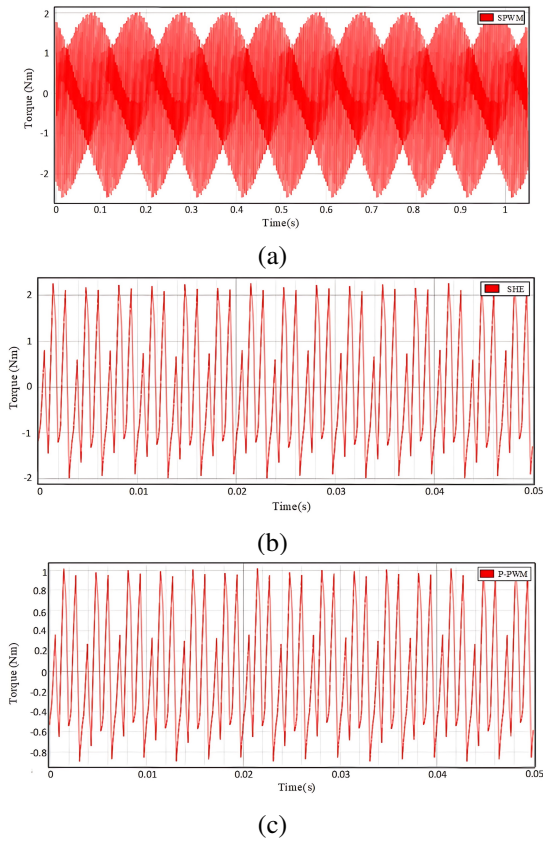
Fig. 6. Torque vibrations (peak to peak) under no loading conditions for (a) $S - PWM$ (b) $SHE - PWM$ (c) SRF-based $P - PWM$.
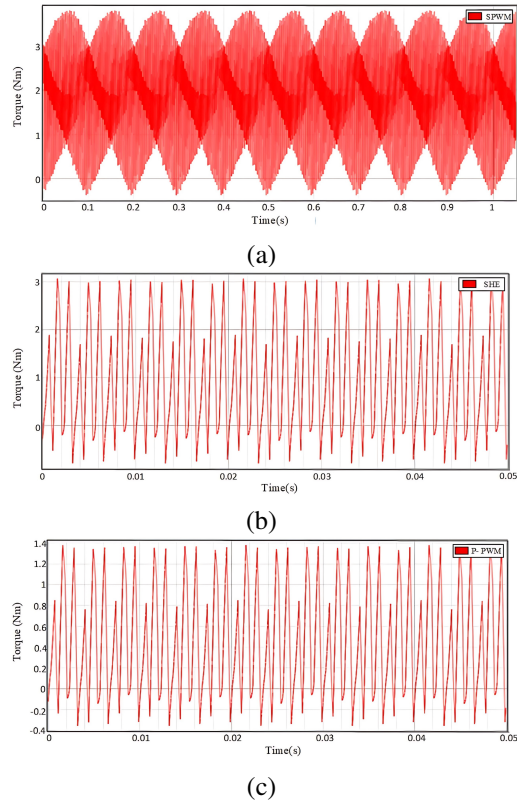

Fig. 7. Torque vibrations (peak to peak) under loading conditions 60% for (a) $S - PWM$ (b) $SHE - PWM$ (c) SRF-based $P - PWM$.

Table 1. Parameters of IM.

Specifications	
Stator Resistances (Rs)	13.12 ohm
Rotor Resistances (Rr)	11.02 ohm
Stator Inductance (Ls)	0.0276 H
Rotor Inductance (Lr)	0.0194 H
Voltage (line-line)	415 V
Mutual Inductance (Lm)	0.3482H
Inertia (J)	0.0331 (kg.m2)
Friction Factor (F)	0.005985 (N.m.s)
Frequency (f)	50
Poles pairs (p)	2

Table 2. Torque vibration (peak to peak) at No load Condition.

PWM Algorithm	Torque (Nm)
S-PWM	4.76
SHE	4.12
SRF based P-PWM	1.82

Table 3. Torque vibration (peak to peak) at 60% loading Condition.

PWM Algorithm	Torque (Nm)
S-PWM	3.87
SHE	3.22
SRF based P-PWM	1.66

Table 4. Torque vibration (peak to peak) for Modulation Index at loading conditions.

Modulation Index (Mo)	SPWM	SHE	SRF based P-PWM
0.1	2.75	2.27	1.18
0.2	3.12	2.55	1.35
0.3	3.61	2.92	1.53
0.4	3.87	3.22	1.66
0.5	4.24	3.41	1.87
0.6	4.57	3.80	1.91
0.7	4.92	3.96	2.09
0.8	5.23	4.26	2.28
0.9	5.45	4.46	2.36

A) Case1. No loading condition

B) Case2. Loading Condition

3.3. TORQUE SPECTRUM ASSESSMENT

The harmonic vibration spectrum primarily represents the magnitude of respective harmonic order concerning fundamental frequency or multiples of the fundamental frequency. In the present section, the Vibration spectrum of torque in inverter-fed IM drive is mainly categorised as in the above-mentioned Cases. Case1 incorporates the No loading conditions listed in Fig. 8. Similarly, for 60% Loading conditions, Case2 is listed in Fig. 9.

Torque output spectrum in inverter-fed IM drive, with $S - PWM$, is listed in Fig. 8-(a). for no loading and Fig. 9-(a) for loading conditions. Similarly, the Output torque spectrum in the inverter fed $SHE - PWM$ based drive is shown in Fig. 8-(b) and Fig. 9-(b). for no loading and loading conditions. Additionally, in Fig. 8-(c) and Fig. 9-(c). The torque output spectrum of the SRF-based $P - PWM$ controlled algorithm in the IM drive is shown at no loading and loading conditions, respectively.

A) Case1. No loading condition

B) Case2. Loading Condition

Analysing the output torque vibration spectrum in both cases, it can be pointed out that for $Sq = 4$, in $S - PWM$ based algorithm, the lowest torque harmonics *i.e.*, 5th corresponding to $250Hz$, followed by 11th and 16th corresponding to $550Hz$ and $800Hz$ are observed in Fig. 8-(a) and Fig. 9-(a). In the $S - PWM$-based IM drive due to a lack of symmetry, both odd and even torque harmonics are observed and shown in a spectrum of no loading and loading conditions. Therefore, the primary comparison of spectrum in inverter fed drive is between
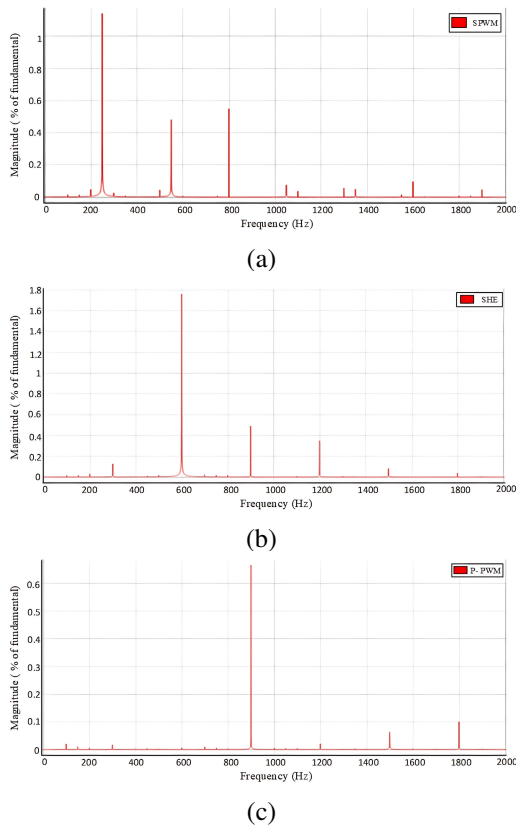
Fig. 8. Spectrum of torque for (a) $S - PWM$ (b) $SHE - PWM$ (c) SRF-based $P - PWM$ under No loading conditions.

Fig. 9. Spectrum of torque for (a) $S - PWM$ (b) $SHE - PWM$ (c) SRF-based $P - PWM$ under 60% loading conditions.

two algorithms, $SHE - PWM$ and SRF-based $P - PWM$. The 12th order is the lowermost harmonic that appears in the torque spectrum corresponding to the frequency $600Hz$ in inverter-fed IM drive using the $SHE - PWM$ algorithm listed in Fig. 8-(b) and Fig. 9-(b). The same 12th-order torque harmonic is nearly eliminated by using SRF-based $P - PWM$ depicted in Fig. 8-(c) and Fig. 9-(c). The harmonic torque spectrum (12th order) corresponding to $600Hz$ frequency is nearly eliminated and alternatively, the higher order harmonic (18th order) corresponding to $900Hz$ is slightly increased using SRF-based $P - PWM$ technique of inverter fed induction motor drive. The elimination of harmonic torque in the proposed SRF-based $P - PWM$ is due to the inclusion of the coupling effect (cross-coupling), which was ignored in earlier studies.

4. CONCLUSION

An SRF-based $P - PWM$ scheme with the machine and load-independent restrictions is proposed for IM drive with $Sq = 4$, $i.e.$, four-time switching per quarter cycle. With the proposed PWM technique, the torque harmonics and vibrations of an IM drive are analysed and extensively compared with standard PWM techniques specifically $S - PWM$ and $SHE - PWM$. In an inverter-fed induction motor drive for $Sq = 4$, the proposed technique can minimize the lowest harmonic torque, that is, the twelfth-order harmonic torque. Apart from harmonic minimization, the torque vibration in the steady state is also reduced by more than 50% in contrast to standard PWM ($S - PWM$ and $SHE - PWM$). Furthermore, the proposed technique is easily extensible for any Sq, higher-order harmonics, and torque vibrations. With the proposed SRF-based $P - PWM$ IM drive will be sturdier to vibration and noises, minimise depreciation of components, increase dr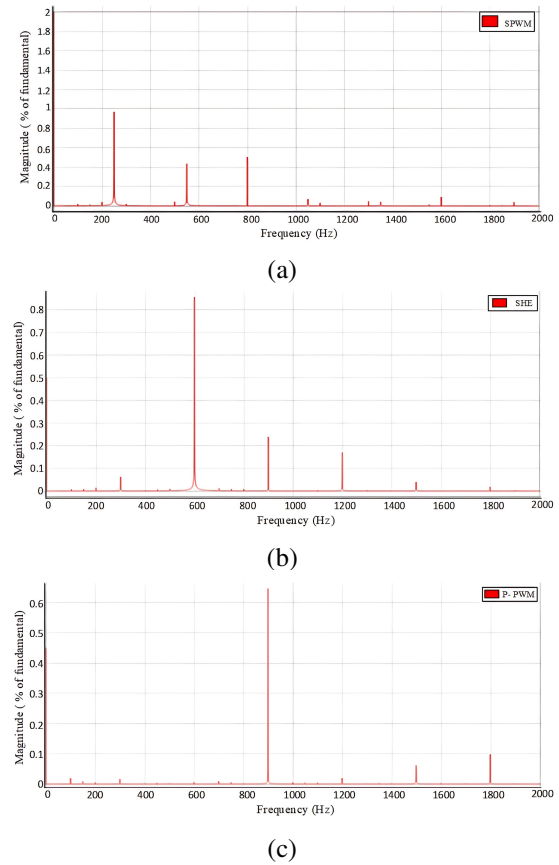ive service life, etc. The proposed schemes stand proven, and verdicts were established both at no loading and loading state through results of real-time and $TYPHOON - HIL$-based hardware setup.

REFERENCES

[1] A. T. D. Almeida, F. J. T. E. Ferreira, and A. Quintino, "Technical and economical considerations on super high-efficiency three-phase motors," 48th IEEE Ind. Commer. Power Syst. Conf., pp. 1-13, 2012.

[2] A. T. D. Almeida, F. J. T. E. Ferreira, and G. Baoming, "Beyond induction motors — Technology trends to move up efficiency," 49th IEEE/IAS Ind. Commer. Power Syst. Tech. Conf., pp. 1-13,2013.

[3] I. Husain et al., "Electric Drive Technology Trends, Challenges, and Opportunities for Future Electric Vehicles," Proc. IEEE, vol. 109, no. 6, pp. 1039-1059, 2021.

[4] M. A. Hannan, J. A. Ali, P. J. Ker, A. Mohamed, M. S. H. Lipu, and A. Hussain, "Switching Techniques and Intelligent Controllers for Induction Motor Drive: Issues and Recommendations," IEEE Access, vol. 6, pp. 47489-47510, 2018.

[5] K. Peter, S. Hanke, F. Mink, and J. Böcker, "Inverter loss management for an electrical high-speed drive system," 2016 18th Eur. Conf. Power Electron. Appl. (EPE'16 ECCE Europe), pp. 1-10,2016.

[6] Y. Wu, M. A. Shafi, A. M. Knight, and R. A. McMahon, "Comparison of the Effects of Continuous and Discontinuous PWM Schemes on Power Losses of Voltage-Sourced Inverters for Induction Motor Drives," IEEE Trans. Power Electron., vol. 26, no. 1, pp. 182-191, 2011.

[7] K. R. Jardan, "Modes of Operation of Three-Phase Inverters," IEEE Trans. Ind. Gen. Appl., vol. IGA-5, no. 6, pp. 680-685, 1969.

[8] J. Vittek and M. Y. Najjar, "Common methodology for steady state harmonic analysis of inverters," IEEE Trans. Power Delivery, vol. 10, no. 3, pp. 1628-1634, 1995.

[9] K. R. Jardan, S. B. Dewan, and G. R. Slemon, "General Analysis of Three-Phase Inverters," IEEE Trans. Ind. Appl. Gen. Appl., vol. IGA-5, no. 6, pp. 672-679, 1969.

[10] H. Dahmardeh, M. Ghanbari, and S. M. Rakhtala, "A Novel Combined DTC Method and SFOC System for Three-phase Induction Machine Drives with PWM Switching Method," (in en), J. Oper. Autom. Power Eng., vol. 11, no. 2, pp. 76-82, 2023.

[11] M. Nikpayam , M. Ghanbari1 , A. Esmaeli and M. Jannati, "Vector Control Methods for Star-Connected Three-Phase Induction Motor Drives Under the Open-Phase Failure," (in en), J. Oper. Autom. Power Eng., vol. 10, no. 2, pp. 155-164, 2022.

[12] P. Naganathan and S. Srinivas, "Direct Torque Control Techniques of Three-Level H-Bridge Inverter Fed Induction Motor for Torque Ripple Reduction at Low Speed Operations," IEEE Trans. Ind. Electron., vol. 67, no. 10, pp. 8262-8270, 2020.

[13] S. Kouro, J. Rebolledo, and J. Rodriguez, "Reduced Switching-Frequency-Modulation Algorithm for High-Power Multilevel Inverters," IEEE Trans. Ind. Electron., vol. 54, no. 5, pp. 2894-2901, 2007.

[14] A. K. Mishra, B. S. Rajpurohit, and R. Kumar, "Revampment of surface permanent magnet synchronous motor design for ameliorated torque profile in e-mobility applications," IET Electr. Syst. Trans., vol. 11, no. 2, pp. 99-108, 2021.

[15] A. K. Mishra, B. S. Rajpurohit, and R. Kumar, "Induction Machine Drive Design for Enhanced Torque Profile," IEEE Transactions on Industry Appl., vol. 54, no. 2, pp. 1283-1291, 2018.

[16] G. B. Kliman and A. B. Plunkett, "Development of a Modulation Strategy for a PWM Inverter Drive," IEEE Trans. Ind. Applications, vol. IA-15, no. 1, pp. 72-79, 1979.

[17] A. Dejamkhooy and A. Ahmadpour, "Torque Ripple Reduction of the Position Sensor-less Switched Reluctance Motors Applied in the Electrical Vehicles," (in en),J. Oper.

[18] A. M. Hava and N. O. Çetin, "A Generalized Scalar PWM Approach With Easy Implementation Features for Three-Phase, Three-Wire Voltage-Source Inverters," IEEE Trans. Power Electron., vol. 26, no. 5, pp. 1385-1395, 2011.

[19] M. S. A. Dahidah, G. Konstantinou, and V. G. Agelidis, "A Review of Multilevel Selective Harmonic Elimination PWM: Formulations, Solving Algorithms, Implementation and Applications," IEEE Trans. Power Electron., vol. 30, no. 8, pp. 4091-4106, 2015.

[20] H. S. Patel and R. G. Hoft, "Generalized Techniques of Harmonic Elimination and Voltage Control in Thyristor Inverters: Part I–Harmonic Elimination," IEEE Trans. Ind. Appl., vol. IA-9, no. 3, pp. 310-317, 1973.

[21] A. Edpuganti and A. K. Rathore, "A Survey of Low Switching Frequency Modulation Techniques for Medium-Voltage Multilevel Converters," IEEE Trans. Ind. Appl., vol. 51, no. 5, pp. 4212-4228, 2015.

[22] M. Hosseinpour, S. Mansoori and H. Shayeghi, "Selective Harmonics Elimination Technique in Cascaded H-Bridge Multi-Level Inverters Using the Salp Swarm Optimization Algorithm," (in en),),J. Oper. Autom. Power Eng., vol. 8, no. 1, pp. 32-42, 2020.

[23] A. Tripathi and G. Narayanan, "Evaluation and Minimization of Low-Order Harmonic Torque in Low-Switching-Frequency Inverter-Fed Induction Motor Drives," IEEE Trans. Ind. Appl., vol. 52, no. 2, pp. 1477-1488, 2016.

[24] A. Tripathi and G. Narayanan, "Evaluation and minimization of low-order harmonic torque in low-switching-frequency inverter fed induction motor drives," IEEE Int. Conf. Power Electron., Drives Energy Syst. (PEDES), pp. 1-6,2014.

[25] A. Tripathi and G. Narayanan, "Torque ripple minimization in neutral-point-clamped three-level inverter fed induction motor drives operated at low-switching-frequency," 2016 Int. Symp. Power Electron, Electr. Drives, Autom. Motion (SPEEDAM), pp. 728-733,2016.

[26] D. W. Grieve and I. E. McShane, "Torque pulsations on inverter fed induction motors," Fourth Int. Conf. Electr. Machines and Drives Conf., pp. 328-333,1989.

[27] B. B.K., Modern Power Electronics and AC Drives. Prentice Hall, 2002.

[28] I. Boldea and S. A. Nasar, Electric drives. CRC press, 2016.